Carbohydrate Polymers 110 (2014) 360–366

Contents lists available at ScienceDirect

Carbohydrate Polymers

journal homepage: www.elsevier.com/locate/carbpol

1D and 2D NMR of nanocellulose in aqueous colloidal suspensions

Feng Jiang[a], Jerry. L. Dallas[b], B. Kollbe Ahn[a], You-Lo Hsieh[a,*]

[a] Fiber and Polymer Science, University of California, Davis, CA95616, USA
[b] NMR Facility, University of California, Davis, CA95616, USA

ARTICLE INFO

Article history:
Received 10 June 2013
Received in revised form 30 January 2014
Accepted 2 March 2014
Available online 27 March 2014

Keywords:
^{1}H NMR
^{13}C NMR
Heteronuclear single quantum coherence (HSQC)
Cellulose nanocrystals
Cellulose nanofibrils

ABSTRACT

This is the first report on surface structural elucidation of individual nanocellulose as colloidal suspensions by 1D ^{1}H, 2D heteronuclear single quantum coherence (HSQC) as well as ^{13}C nuclear magnetic resonance (NMR). ^{1}H NMR of rice straw CNCs (4.7 nm thick, 143 nm long, 0.04 sulfate per AG or 19.0% surface hydroxyl to sulfate conversion) resembled that of homogeneous cellulose solution. Conventional 2D HSQC NMR of CNC, CNF 1.5 (2–14 nm thick, several micrometers long, 0.10 —COOH per AG) and CNF10 (2.0 nm thick, up to 1 μm long, 0.28 —COOH per AG) gave H1:H2 ratios of 1.08:1, 0.97:1 and 0.94:1, respectively, all close to the theoretical 1:1 value for cellulose. The H1:H6 ratios determined from 2D HSQC NMR for CNCs, CNF1.5 and CNF10 were 1:1.47, 1:0.88 and 1:0.14, respectively, and corresponded to 26%, 56% and 93% C6 primary hydroxyl conversion to sulfate and carboxyl groups, consistent with, but more sensitive than those by conductometric titration and X-ray diffraction. Both ^{1}H and 2D HSQC NMR data confirm that solution-state NMR detects nanocellulose surface carbons and protons primarily, validating this technique for direct surface characterization of nanocellulose in aqueous colloidal suspensions, presenting a sensitive and meaningful NMR tool for direct characterizing individual nanocellulose surfaces in never-dried state.

1. Introduction

Nanocellulose, the nano-scale fibrillar crystalline domains derived from cellulose, has attracted significant attention due to their ultra-high strength and modulus, low thermal expansion coefficient in the axial direction, high specific surface, chemical reactivity and low densities (Habibi, Lucia, & Rojas, 2010; Isogai, Saito, & Fukuzumi, 2011; Klemm et al., 2011). Nanocellulose has been commonly derived by chemical or mechanical means, including acid hydrolysis (Beck-Candanedo, Roman, & Gray, 2005; Jiang, Esker, & Roman, 2010), 2,2,6,6-tetramethylpyperidine-1-oxyl (TEMPO) mediated oxidation (Saito & Isogai, 2004), biochemical enzymatic hydrolysis (Paakko et al., 2007), mechanical defibrillation (Uetani & Yano, 2011) or a combination of the above, in the form of aqueous suspensions. Structural characterization of nanocellulose, however, has been mainly carried out on their solids by well-developed solid state techniques such as Fourier transform infrared spectroscopy (FTIR) (Araki, Wada, & Kuga, 2001), X-ray photoelectron spectroscopy (XPS) (Jiang et al., 2010; Yuan, Nishiyama, Wada, & Kuga, 2006), energy-dispersive X-ray spectroscopy (EDX) (Lu & Hsieh, 2011) and solid-state ^{13}C nuclear magnetic resonance (NMR) (Berlioz, Molina-Boisseau, Nishiyama, & Heux, 2009; Cetin et al., 2009). Nanocellulose is widely known to agglomerate during drying, therefore solid-state characterization may reflect certain structural changes from drying and not necessarily the precise nature of the individual nanocellulose.

Solution-state NMR gives specific structural information of individual molecules and is commonly used to determine chemical changes of cellulose and degree of substitution of cellulose derivatives, all in soluble forms. Solution-state NMR has only been reported on soluble or hydrolysis products of cellulose, such as ^{1}H and ^{13}C NMR of water-soluble polyglucuronic acid derived from TEMPO oxidized cellulose (Hirota, Tamura, Saito, & Isogai, 2009; Tahiri & Vignon, 2000) and ^{1}H and 2D NMR of hydrolyzed monosaccharides of cationized nanocrystalline cellulose (de la Motte, Hasani, Brelid, & Westman, 2011). To date, solution-state NMR of nanocellulose in colloidal suspensions has not been reported.

Solution-state ^{1}H and ^{13}C NMR have also shown to be effective for analyzing molecules adsorbed on the surface of carbon nanotube (Huang, Fernando, Allard, & Sun, 2003; Sun, Fu, Lin, & Huang, 2002; Tang & Xu, 1999) and gold nanoparticles (Hostetler et al., 1998; Terrill et al., 1995; Zhou et al., 2008), although the resolved peaks are broader than those of same molecules in the soluble form. Similarly, nanocellulose can be considered as nanoparticles

* Corresponding author. Tel.: +1 530 752 0843; fax: +1 530 752 7584.
E-mail address: ylhsieh@ucdavis.edu (Y.-L. Hsieh).

http://dx.doi.org/10.1016/j.carbpol.2014.03.043
0144-8617/

with highly crystalline cellulose cores and functionalized shells. Nanocellulose also has nano-scale lateral dimensions and aspect ratios approaching some of the largest macromolecules. It is, therefore, hypothesized that solution-state NMR may be appropriate for surface structural characterization of nanocellulose.

In this study, nanocellulose of different dimensions and surface chemistries was probed using solution-state 1D and 2D NMR to determine their suitability for direct characterizing the surfaces of individual nanocellulose in colloidal suspensions. Nanocellulose was prepared by either sulfuric acid hydrolysis or coupled TEMPO oxidation and blending to varied dimensions and surface chemistries and maintained as aqueous suspensions for characterization. Integrals of 2D heteronuclear single quantum coherence (HSQC) NMR were used to determine the degree of surface oxidation of primary hydroxyls and compared with conductometric titration and X-ray diffraction data.

2. Experimental

2.1. Derivation and characterization of cellulose nanocrystals (CNCs) and nanofibrils (CNFs)

Pure cellulose was isolated from rice straw (Calrose varity) and hydrolyzed into CNCs (64 wt% sulfuric acid, 8.75 mL/g acid-to-cellulose ratio, 45 °C, 45 min) as previously reported (Lu & Hsieh, 2011). CNF1.5 and CNF10 were derived from TEMPO mediated oxidation of rice straw cellulose at 1.5 and 10 mmol/g NaClO/cellulose, then blended at 37,000 rpm for 60 and 30 min, respectively, following a previous procedure (Jiang, Han, & Hsieh, 2013).

CNCs and CNFs were characterized as suspensions and freeze-dried solids as previously described (Jiang & Hsieh, 2013; Jiang et al., 2013). The surface charges were determined by conductometric titration of 0.1 wt% suspensions. Individual CNCs and CNFs were visualized using an Asylum-Research MFP-3D atomic force microscope (AFM). The transverse and longitudinal dimensions of CNCs and CNFs were determined from AFM images and reported as means and standard deviations. The transverse dimensions were calculated from the heights of 150 images where the z resolution was 0.06 nm. The lengths in the direction parallel to the long axis are sufficiently long to negate the tip broadening effect. CNCs and CNFs were freeze-dried to be measured on a Scintag XDS 2000 powder diffractometer (XRD) to calculate crystallinity index (CrI) and crystallite dimensions. CrI was calculated from the intensity of the 200 peak (I_{200}, $2\theta = 22.6^\circ$) and the intensity minimum between the 200 and 110 (I_{am}, $2\theta = 18.7^\circ$) peaks by using the empirical equation, $\mathrm{CrI} = (I_{200} - I_{am})/I_{200} \times 100$ (Segal, Creely, Martin, & Conrad, 1959). The primary C6 hydroxyls on CNF surfaces (mol per mol of AG, OH/AG) were determined using a method reported previously (Jiang et al., 2013; Okita, Saito, & Isogai, 2010)

2.2. NMR

CNC and CNF suspensions (around 10 mL at 0.6 wt%) were precipitated by adding 40 mL acetone then centrifuged (5000 rpm, 15 min) to decant the supernatant and repeated three times. A fraction of CNC and CNF acetone gels was added into 1 mL D_2O, and was dispersed by sonication (10 min, Branson 2510), followed by heating at 60 °C under vacuum for 1 h to remove acetone. This sonication and evaporation process was repeated several times to remove residual acetone and additional D_2O was added during evaporation to prevent drying. The final nanocellulose concentration was around 0.2 wt%.

^{1}H, ^{13}C and 2D HSQC NMR spectra and ^{1}H spin-lattice relaxation time measurements were carried out using a Bruker AVIII 600 MHz spectrometer using a 5 mm CPTCI H/C/N/D Z-gradient cryogenic probe. Spin-lattice relaxation time T1 was measured using saturation recovery pulse sequence ($\pi/2$–T_R–$\pi/2$), where T_R is the saturation recovery time, ranging from 150 to 7000 ms. The area of each peak was used for the relaxation curve fitted by an mono-exponential function, $I(T_R) = I(1-\exp(-T_R/\mathrm{T1}))$. Proton spectra were obtained at 303 K in deuterium oxide (99.96% D) solvent with the NOESYPR1D experiment. A presaturation field strength of 50 Hz was applied to the H_2O resonance during a 5 s predelay followed by a 90° acquisition pulse and acquisition time of 1 s. The mixing time was 100 ms. Typical conditions employed eight dummy pulses and eight scans. Carbon spectra employed a 45° tip angle with a 1.5 s (D1 = 0.5 s, AQ = 1 s) repetition rate for a total acquisition time of 1 h with GARP decoupler modulation, and no inverse gated decoupling. 2D heteronuclear correlation experiments employed the HSQCETGPSP.2. Bruker standard experiment using 2 K × 128 complex data points in T2 and T1 with echo/antiecho data collection and processing in pure phase. Spectral widths were 16 × 165 ppm with variable scans per block according to time constraints (44, 80, and 112 scans for CNC, CNF1.5 and CNF10, respectively). For each sample, the delay time was set to at least 5 times of the longest T1. Processed data were zero filled to 2 K × 1 K with linear prediction in T1 of 768 points. Apodization was cosine square bell in both dimensions (SSB = 2). ^{13}C decoupler modulation during acquisition featured CPD = bi_p5m4sp.2. For the integral of 2D HSQC results, the proton at the anomeric carbon (H1), which is not affected by sulfuric acid hydrolysis or TEMPO oxidation, was employed as an internal standard and the relative integral ratios were reported. (Ahn, Kraft, & Sun, 2011)

3. Results and discussion

3.1. Morphologies and surface properties of nanocellulose

Rice straw cellulose was hydrolyzed into rigid rod-like CNCs, averagely 4.7 (±1.3) nm thick and 143 (±31) nm long (Fig. 1a and d) (Jiang & Hsieh, 2013). Coupled TEMPO mediated oxidation and mechanical blending yielded 97% CNFs out of the starting rice straw cellulose, with morphologies depending on the degree of oxidation (Jiang et al., 2013). The CNF1.5, isolated at 1.5 mmol NaClO/g of cellulose, were 2–14 nm thick and several micrometers long, showing bimodal distributed thin and thick nanofibrils (Fig. 1b and e). Oxidized at a higher 10 mmol NaClO/g of cellulose, CNF10 measured averagely 2.0 (±0.7) nm thick and from hundreds to thousands nanometers long (Fig. 1c and f).

Isolating nanocellulose under strongly acidic and highly oxidative conditions causes not only defibrillation and chain scissions but also chemical modification of the surface hydroxyls. The hydroxyls on CNCs are semi-esterified during sulfuric acid hydrolysis whereas the C6 primary hydroxyls are oxidized to carboxyls on CNF surfaces from TEMPO mediated oxidation. The negatively charged sulfates on CNCs and carboxyls on CNFs were confirmed and quantified by conductometric titration to be 0.24, 0.59 and 1.68 mmol/g of cellulose, equivalent to 0.04, 0.10 and 0.28 DS values per anhydroglucose (AG) unit (Fig. 1g) for CNC, CNF1.5 and CNF10, respectively.

The derived nanocellulose are highly crystalline with CrI of 90.7%, 70.8%, and 84.8% for CNC, CNF1.5 and CNF10, respectively. The increased crystallinities for CNC and CNF10 as compared with the original rice straw cellulose (72.2% CrI) are expected from the removal of less ordered cellulose chains by the extensive acid hydrolysis and oxidation reaction, manifesting these chemical conversions to be limited to the crystal surfaces. The average crystallite size of CNCs from XRD is 4.3 nm (Fig. 1g), very close to their average 4.7 nm lateral dimension by AFM. The average crystallite sizes of 3.0 and 2.6 nm for CNF1.5 and CNF10 are also approximate to their respective 2–14 and 2.0 nm lateral dimensions,

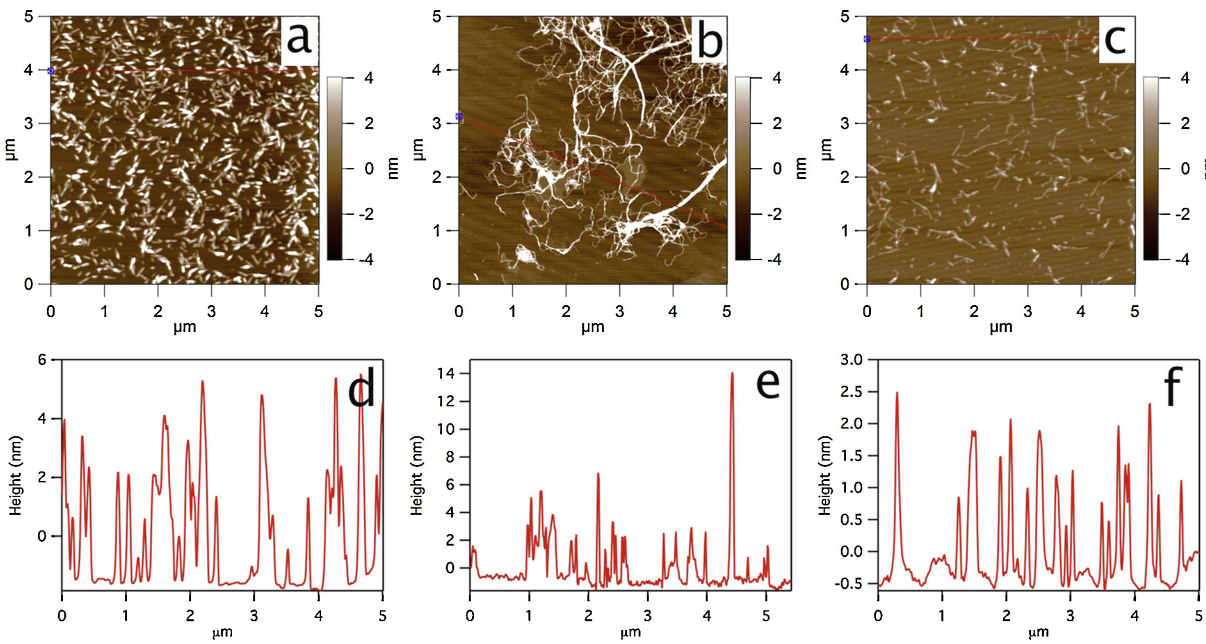

g

Samples		CNC	CNF1.5	CNF10
Crystallite dimension (nm)	$1\bar{1}0$	4.0	2.6	2.5
	110	4.6	3.4	2.7
	Average	4.2	3.0	2.6
Surface C6 primary hydroxyls (OH/AG)		0.21	0.27	0.30
DS (charge/AG)		0.04	0.10	0.28
Surface hydroxyl substitution (%)		19.0	37.0	93.3

Fig. 1. AFM height images (a–c) and height profiles (d–f): (a, d) CNC; (b, e) CNF1.5; (e, f) CNF10; (g) Crystallite dimension, surface primary hydroxyls, degree of substitution (DS) and surface hydroxyl substitution of CNCs, CNF1.5 and CNF10. The DS is calculated from $DS = (q \times MW_a)/(1 + q \times (MW_a - MW_{b\,or\,c}))$; where MW_a, MW_b and MW_c are the molecular weights of anhydroglucose ($C_6H_{10}O_5$, 162 g/mol), anhydroglucuronic acid ($C_6H_8O_6$, 176 g/mol) and anhydroglucose sulfate ($C_6H_{10}O_8S$, 242 g/mol), respectively, and q is the charge density determined from conductometric titration in mol/g.

suggesting their highly crystalline cores. Within the crystalline core of these nanocellulose, the hydroxyls are intra- and intermolecularly hydrogen bonded while only the surface ones are accessible and reactive. The theoretical quantities of surface C6 primary hydroxyls on CNC, CNF1.5 and CNF10 are calculated from their crystallite dimensions to be 0.21, 0.27 and 0.30 OH/AG, respectively (Fig. 1g) (Jiang et al., 2013). The proportions of the surface C6 hydroxyls that were substituted were calculated by dividing the 0.04, 0.10 and 0.28 DS values derived from conductometric titration by the original surface C6 primary hydroxyls derived from XRD to be 19.0%, 37.0% and 93.3% for CNC, CNF1.5 and CNF10, respectively (Fig. 1g).

3.2. NMR characterization of nanocellulose

Proton spin-lattice relaxation time (T1) reflects the recovery rate of the longitudinal component of the magnetization vector toward thermodynamic equilibrium, and is affected by solvent, temperature, nuclear environment and molecular motion, etc. T1s of all nanocellulose were measured in D_2O using saturation recovery pulse sequence, and calculated using a monoexponential function, representing the time required for 63% of magnetization to recover to equilibrium. From the saturation recovery curves of H2 (Fig. 2a), it shows that the recovery is slowest for CNCs, followed by CNF1.5 and CNF10, with calculated T1s being 1.83, 1.05, and 0.44 s, respectively (Fig. 2b). This decreasing T1 trend is consistent with the decreasing lateral dimensions of these nanocellulose. The longer T1 for CNCs could be due to their wider lateral dimension and higher crystallinity, rendering slow tumbling and reorienting of the large molecules. For CNF1.5, the lateral dimensions are much smaller and the crystallinity is lower, therefore the molecular motions are more rapid to generate shorter T1. As expected, CNF10 showed shortest T1 due to its much smaller lateral and longitudinal dimensions as compared to CNF1.5. The T1s for H6 are much shorter than those for H2 for both CNC (0.61 s) and CNF1.5 (0.42 s) (Fig. 2b), which could be due to faster internal motion as they are attached to the

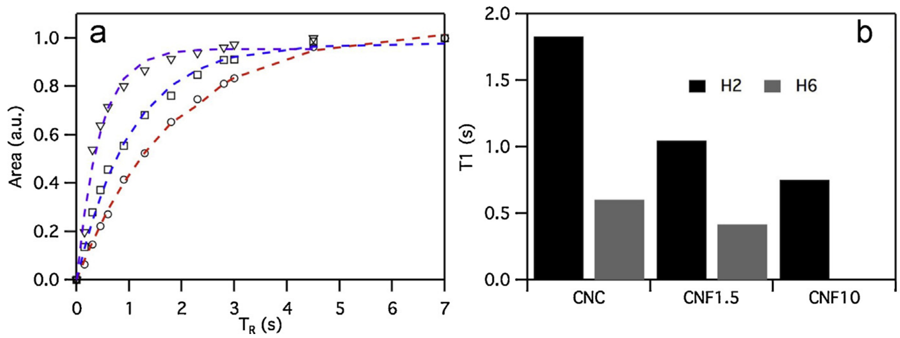

Fig. 2. (a) Saturation recovery curves of H2 for CNC (○), CNF1.5 (□), and CNF10 (△), dash lines are fitting curves calculated from monoexponential function $I(T_R) = I(1 - \exp(-T_R/T1))$; (b) Spin-lattice relaxation T1 of H2 and H6.

secondary carbon. T1 for H6 in CNF10 could not be determined due to its absence, i.e., oxidation of C6 methylene groups to carbonyl group.

Solution-state ^{1}H NMR (Fig. 3) was obtained from never-dried nanocellulose/D_2O, i.e., solvent exchanged from aqueous suspension, to avoid drying and possible agglomeration. For all nanocellulose/D_2O suspensions, clear ^{1}H NMR spectra were obtained in less than 2 min, indicating nanocellulose to remain well dispersed in D_2O after H_2O–acetone–D_2O solvent exchange process, behaving like soluble macromolecules. For the CNC/D_2O suspension (Fig. 2a), the furthest downfield peaks at δ 4.45 could be assigned to the proton at the anomeric carbon (H1), which is in close approximation to the previously reported chemical shift values of H1 in dissolved cellulose, i.e., δ 4.5 for cellulose/NaOD/D_2O system (Kowsaka, Okajima, & Kamide, 1988), δ 4.6 for cellulose/N,N-dimethylacetamide-d_9/LiCl (Nardin & Vincendon, 1986), δ 4.35 for cellulose/dimethyl sulfoxide-d_6 (Buchanan, Edgar, Hyatt, & Wilson, 1991). The doublet peaks present at δ 3.90 and δ 3.75 for CNC could be assigned to the methylene protons or H6 and are consistent with the previous reported δ 3.65–3.88 in cellulose/NaOD/D_2O (Isogai, 1997). The appearance of doublet is from the spin–spin coupling between the two vicinal protons. The plural peaks between δ 3.34 and 3.66 are from the three C3, C4 and C5 protons, but impractical to separate due to their significant overlapping with each other. The furthest upfield peak at δ 3.27 coincides with the chemical shift of H2 and is consistent with the previous reported δ 3.29 for cellulose/NaOD/D_2O (Kowsaka et al., 1988), δ 3.05 for cellulose/DMA-d_9/LiCl (Nardin & Vincendon, 1986) and δ 4.10 for cellulose/dimethyl sulfoxide-d_6 (Buchanan et al., 1991).

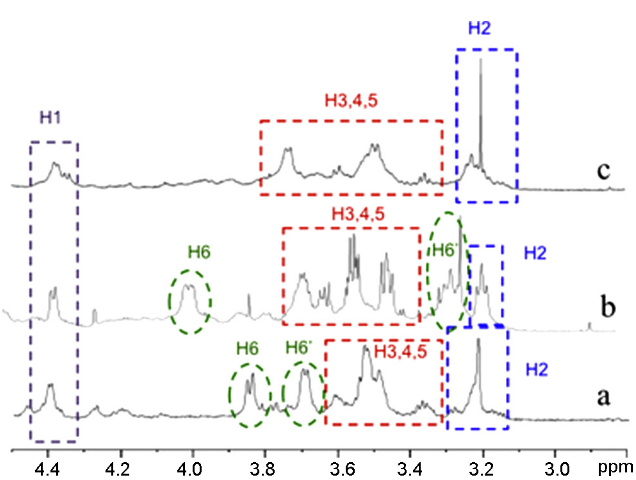

Fig. 3. ^{1}H NMR spectra of nanocellulose in D_2O suspension: (a) CNC; (b) CNF1.5; (c) CNF10.

The ^{1}H peak assignment for CNC/D_2O was further confirmed with 2D ^{1}H–^{13}C HSQC spectrum (Fig. 4a), offering one-bond correlation between carbon and proton. The projection of ^{13}C spectrum correlated with the proton nuclei was shown on the vertical axis and the projection of ^{1}H spectrum correlated with the carbon nuclei was shown on the horizontal axis. The well resolved ^{13}C NMR spectrum of cellulose had shown the most deshielded anomeric carbon at δ 102.00, followed by a less deshielded carbon C4 at δ 79.00–80.00 and the most shielded methylene carbon C6 at δ 60.00, with other C2, C3, and C5 signals at around δ 74.00 (Bain, Eaton, Hux, & Tong, 1980; Elkafrawy, 1982; Nehls, Wagenknecht, Philipp, & Stscherbina, 1994). The H1 at δ 4.45 was coupled with anomeric C1 at δ 102.1. The H6 signals at δ 3.90 and 3.75 were coupled with the primary methylene C6 at δ 59.8. The H4 at δ 3.58 correlated with C4 at δ 78.5 whereas the H2 at δ 3.27 with C2 at δ 72.8. The two overlapping contour peaks of H3 and H5 at δ 3.55 were coupled with C3 and C5 at δ 74.2. Essentially, the ^{1}H NMR spectrum for CNC/D_2O suspension display significant resemblance to that of homogeneous cellulose solutions (Gagnaire, Mancier, & Vincendon, 1980) and the chemical shift values from both ^{1}H and 2D HSQC NMR spectra coincide well with the reference data. This observation indicates that solution ^{1}H and 2D HSQC NMR are suitable for resolving chemical structures of CNC in suspensions. Previous ^{1}H magic angle spinning (MAS) NMR of swollen cellulose nanowhiskers in D_2O showed only a broad and unresolved peak centered at δ 3.5, which has no structural meaning (Goetz, Foston, Mathew, Oksman, & Ragauskas, 2010). To the best of our knowledge, this is the first report of structural elucidation by solution-state 1D ^{1}H and 2D NMR of aqueous nanocellulose suspensions.

TEMPO oxidation liberates cellulose nanofibrils containing some surface carboxyls converted from C6 primary hydroxyls, thus should display such effect in its NMR spectra. ^{1}H NMR spectra show clear H1 (δ 4.41) and H2 (δ 3.26) peaks for CNF1.5 and CNF10 (Fig. 3b and c), correlating with ^{13}C chemical shifts at δ 101.9 and δ 72.6 from the HSQC spectra for C1 and C2, respectively (Fig. 4b and c). For CNF1.5, two peaks at δ 3.88 and 3.74 were coupled with the C6 at δ 59.8, which are similar to that for CNCs. Another two peaks at δ 4.04 and 3.30 coupled with C at δ 62.6 were also thought to be from C6. The shifting of these two C6 and H6 peaks of CNF 1.5 was thought to be due to the strong hydrogen bond between the non-oxidized C6 OH and the C6 carbonyl O of partially oxidized CNF 1.5 (Abraham & Mobli, 2007; Ajami et al., 2011; Grzesiek, Cordier, Jaravine, & Barfield, 2004; Moulthrop, Swatloski, Moyna, & Rogers, 2005). Other peaks present in CNF1.5 were assigned as follows: H3 at δ 3.75, C3 at δ 75.7, H4 at δ 3.66, C4 at δ 80.1, H5 at δ 3.52; C5 at δ 74.2. For CNF10, it was clear that the proton signals coupled with C6 at δ 60 (Fig. 4c) disappeared completely as compared to CNC (Fig. 4a) and CNF 1.5 (Fig. 4b). This is expected from losing C6 protons on the surface C6 methylene groups to TEMPO oxidation. It should be noted that 93.3% surface C6 primary

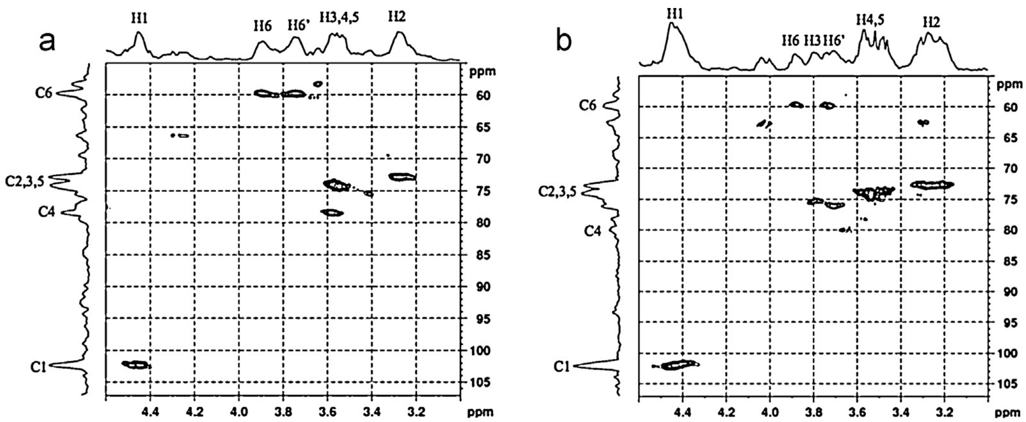

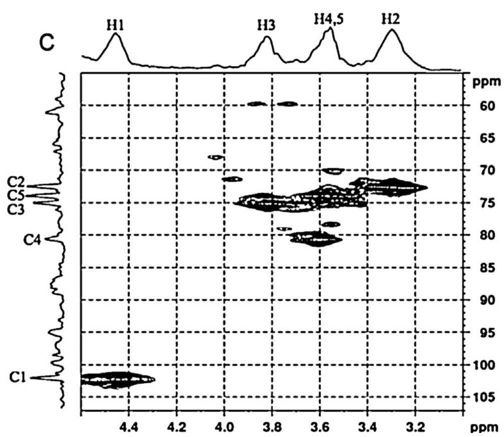

d

	Samples	CNC	CNF1.5	CNF10	Cellulose
Integrals	H1	0.676	0.802	0.854	1
	H2	0.727	0.775	0.802	1
	H6	0.997	0.703	0.122	2
Ratios	H1:H6	1:1.47	1:0.88	1:0.14	1:2
	H1:H2	1.08:1	0.97:1	0.94:1	1:1

Fig. 4. ^{1}H–^{13}C HSQC spectra of nanocellulose in D_2O suspension. (a) CNC; (b) CNF1.5; (c) CNF10; (d) integrals and ratios of proton determined from 2D HSQC NMR spectra. The values for cellulose are from theoretical calculation.

hydroxyl-to-carboxyl conversion is equivalent to only 28% conversion counting all C6 hydroxyls in the CNFs, i.e., including those in the crystalline core (Fig. 1g). In other words, over 70% of the C6 primary hydroxyls resided within the crystalline cellulose fibrils and are unreacted. The fact that almost no C6 and H6 peaks were detected manifests that only the surface nuclei could be detected by NMR of the nanocellulose suspensions. Cellulose chains in the crystalline cores participate in inter- and intra-molecular hydrogen bonding with each other, thus have restricted molecular mobility. Surface chains, having far less constraint than those in the interior, exhibit higher molecule motions that average out the dipolar interaction between neighboring spins. That only the surface structure of nanocellulose in colloidal suspension is detected is another significant finding, confirming solution-state NMR to be an effective and efficient method for surface characterization of nanocellulose in colloidal suspensions. This new finding presents huge advantage for the direct characterization of nanocellulose surface structures as a result of isolation processes and/or modification. Other peaks present in CNF10 could be assigned as: H1 at δ 4.47, C1 at δ102.3, H3 at δ 3.84, C3 at δ 75.2, H4 at δ 3.61, C4 at δ 80.7, H5 at δ 3.57, C5 at δ 74.0. The signal-to-noise ratios of ^{13}C in 2D HSQC (Fig. 4) and ^{13}C NMR (Fig. 5) are much higher for CNF1.5 and CNF10 than for CNCs. This may be attributed to the much narrower and more flexible CNFs, experiencing faster isotropic motion as compared to the wider and more rigid CNCs.

As the delay time used for HSQC measurements are at least 5 times of the longest T1, it is deemed accurate to integrate the contours for quantitative analysis with uncertainty of ±5%. The H1 at the anomeric carbon was used as internal standard and the ratios of other protons relative to H1 were reported (Fig. 4d). The integrals determined from 2D HSQC NMR spectra show the H1:H2 ratio to be 1.08:1, 0.97:1 and 0.94:1 for CNC, CNF1.5 and CNF10, respectively, close to the theoretical 1:1 value for cellulose (Fig. 4d). The H1:H6 for CNC is 1:1.47, ca. 26% lower H6 intensity as compared to cellulose with theoretical 1:2 value. The reduced H6 intensity observed on CNC is attributed to the conversion of some primary hydroxyls to sulfate groups. Actually, the 26% primary hydroxyls

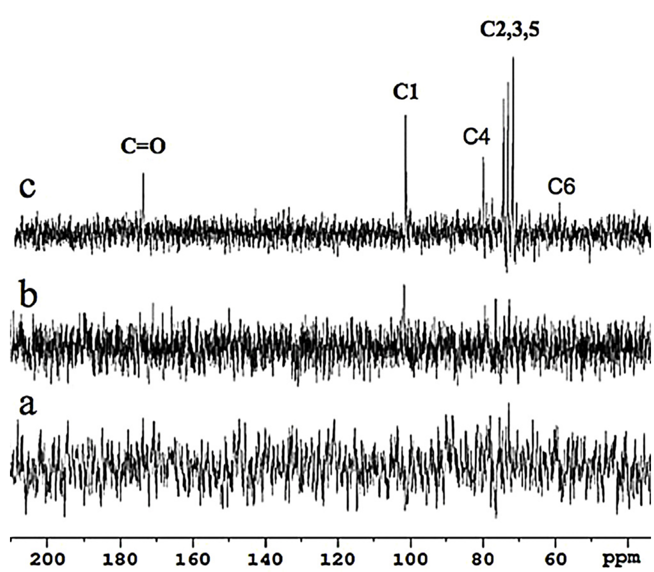

Fig. 5. ^{13}C NMR spectra of nanocellulose in D_2O suspension: (a) CNC; (b) CNF1.5; (c) CNF10.

to sulfate conversion from 2D HSQC is higher than the 19.0% of surface sulfate group conversion derived from conductometric titration and XRD. As expected, lower H6 integrals were also observed for both CNF1.5 and CNF10, resulting from oxidation of the primary C6 hydroxyl. The ratios between H1 and H6 were 1:0.88 and 1:0.14 for CNF1.5 and CNF10, respectively, showing unreacted H6 in these CNFs to be only 44% and 7% of pure cellulose. In other words, 56% and 93% of the primary C6 hydroxyls were converted to carboxyls for CNF1.5 and CNF10, respectively. The hydroxyl-to-carboxyl conversion derived from NMR for CNF1.5 is higher (56%) than the 37.0% value determined by conductometric titration and XRD; whereas the 93% hydroxyl-to-carboxyl conversion for CNF10 is significantly close to the 93.3% value as determined from conductometric titration and XRD (Fig. 1g). With both CNC and CNF1.5, the lower conversion values from conductometric titration and XRD than 2D HSQC NMR was thought to be due to the use of average crystallite dimensions for the widely different sized nanocellulose, thus may be less accurate the NMR approach. Both ^{1}H and 2D HSQC NMR data confirm that solution NMR detects nanocellulose surface carbons and protons primarily and quantitatively, validating this technique for direct surface characterization of nanocellulose in colloidal suspensions.

^{13}C NMR spectrum of CNF10 shows five sharp peaks at δ 103, 81, 75, 74 and 72.5, corresponding to C1, C4, C3, C5 and C2 in cellulose, respectively (Fig. 4c). These results correspond well with 2D HSQC. A small peak could be detected at δ 60, albeit with significantly reduced intensity, indicating conversion of primary methylene carbon to carbonyl carbon which was further confirmed by a new peak near δ 175. Solution ^{13}C NMR of dissolved cellulose has shown the same chemical shifts, but much broader peaks (Elkafrawy, 1982; Moulthrop et al., 2005; Nehls et al., 1994). Solid-state ^{13}C NMR of TEMPO oxidized nanocellulose also exhibited a carbonyl peak at δ 174.8 but much broader peaks for all other carbons (Fujisawa, Okita, Saito, Togawa, & Isogai, 2011; Mao, Ma, Law, Daneault, & Brouillette, 2010; Montanari, Rountani, Heux, & Vignon, 2005; Shibata & Isogai, 2003). The ^{13}C NMR spectra for CNF10 also resembles the solution ^{13}C NMR of water-soluble polyglucuronic acid (Hirota et al., 2009; Tahiri & Vignon, 2000), even though CNFs are highly crystalline solids in colloidal suspensions and with only 28% of primary C6 hydroxyls converted to carboxyls. Therefore, the ^{13}C NMR spectra manifest that cellulose nanofibrils with 2 nm or smaller diameters behave like single cellulose molecules whose surface structure could be analyzed by ^{13}C NMR.

However, the ^{13}C NMR of CNF1.5 showed only very weak signals in the regions of δ 70–105, hardly separated from the background noise (Fig. 5b), while no ^{13}C NMR signals were detected for CNC (Fig. 5a). This indicates that ^{13}C NMR is very sensitive to the surface chemistry of nanocellulose with 2 nm or smaller lateral dimensions where each surface carbon could be detected. In other words, at 2 nm or smaller widths, individual nanocellulose is detected the same as single cellulose chains in ^{13}C NMR. As nanocellulose lateral dimension increases, specific surface reduces, lowering surface carbon atoms, the ^{13}C signals on nanocellulose surfaces reduce to be indistinguishable from the background noise in ^{13}C NMR spectra. Besides, the sensitivity of ^{13}C is considerably less than that of ^{1}H NMR due to the much smaller gyromagnetic ratio (one quarter of ^{1}H) and far lower natural abundance (1.1% for ^{13}C, and 99.985% for ^{1}H). Therefore, ^{13}C is highly sensitive for surface structural analysis of nanocellulose that are 2 nm or smaller in width, but is not suitable for nanocellulose wider than 2 nm due to reduced surface carbon atoms and less natural abundance of ^{13}C. It should also be noted that although almost no ^{13}C signal could be detected from ^{13}C spectra for CNF1.5 and CNC, clear spectra of those carbon coupled with protons could be detected from the 2D proton-detected HSQC spectra (Fig. 4). Proton-detection offers HSQC more intrinsic sensitivity as compared to ^{13}C NMR or other carbon-detected 2D NMR, making HSQC a preferential choice for investigating surface structures of nanocellulose.

4. Conclusions

Surface chemistries of cellulose nanocrystals (CNCs) and nanofibrils (CNFs) of varied dimensions and degrees of surface sulfation and oxidation have been successfully elucidated by solution NMR of their aqueous colloidal suspensions for the first time. ^{1}H NMR of rice straw CNCs (4.7 nm thick, 143 nm long, 0.04 sulfate per AG or 19.0% surface hydroxyl to sulfate conversion) resembled that of dissolved cellulose. Conventional 2D HSQC spectra of CNC, CNF 1.5 (2–14 nm thick, several micrometers long, 0.10 —COOH per AG) and CNF10 (2.0 nm thick, up to 1 μm long, 0.28 —COOH per AG) gave H1:H2 ratios of 1.08:1, 0.97:1 and 0.94:1, respectively, all close to the theoretical 1:1 value for cellulose. The H1:H6 ratio for CNCs was 1:1.47 as compared to the 1:2 ratio for cellulose and the lower H6 was attributed to esterification of the primary hydroxyls. The 1:0.88 H1:H6 value for CNF1.5 corresponded to ca. 56% OH-to-COOH conversion, higher than the 37% value by conductometric titration whereas the 1:0.14 H1:H6 ratio for CNF10 represented 93% OH-to-COOH conversion, very close to the 93.3%. The C6 primary hydroxyl conversion derived from 2D HSQC NMR consistent with, but more sensitive than, those by conductometric titration and X-ray diffraction. The ^{13}C NMR spectrum of CNF10 showed weakened signal at C6 (δ 60) and a new peak at δ 175, both clearly evident of the carbonyl carbon from TEMPO oxidation of cellulose, indicating solution-state ^{13}C NMR to be suitable for only nanocellulose thinner than 2 nm. These findings confirm that solution-state NMR under prescribed preparation and conditions provides direct surface analysis of ultra-fine nanocellulose in aqueous colloidal suspensions, presenting a useful tool for surface characterization of individual nanocellulose in never-dried state.

Acknowledgements

Authors acknowledge California Rice Research Board (Project RU-9) and USDA/NIFA for financial support as well as the UC Davis NMR facility and NSF DBIO722538 and NIH RR11978 instrumentation grants.

References

Abraham, R. J., & Mobli, M. (2007). An NMR IR and theoretical investigation of H-1 chemical shifts and hydrogen bonding in phenols. *Magnetic Resonance in Chemistry*, *45*(10), 865–877.

Ahn, B. J. K., Kraft, S., & Sun, X. S. (2011). Chemical pathways of epoxidized and hydroxylated fatty acid methyl esters and triglycerides with phosphoric acid. *Journal of Materials Chemistry*, *21*(26), 9498–9505.

Ajami, D., Tolstoy, P. M., Dube, H., Odermatt, S., Koeppe, B., Guo, J., et al. (2011). Encapsulated carboxylic acid dimers with compressed hydrogen bonds. *Angewandte Chemie-International Edition*, *50*(2), 528–531.

Araki, J., Wada, M., & Kuga, S. (2001). Steric stabilization of a cellulose microcrystal suspension by poly(ethylene glycol) grafting. *Langmuir*, *17*(1), 21–27.

Bain, A. D., Eaton, D. R., Hux, R. A., & Tong, J. P. K. (1980). An NMR-study of the interactions between cadoxen and saccharides. *Carbohydrate Research*, *84*(1), 1–12.

Beck-Candanedo, S., Roman, M., & Gray, D. G. (2005). Effect of reaction conditions on the properties and behavior of wood cellulose nanocrystal suspensions. *Biomacromolecules*, *6*(2), 1048–1054.

Berlioz, S., Molina-Boisseau, S., Nishiyama, Y., & Heux, L. (2009). Gas-phase surface esterification of cellulose microfibrils and whiskers. *Biomacromolecules*, *10*(8), 2144–2151.

Buchanan, C. M., Edgar, K. J., Hyatt, J. A., & Wilson, A. K. (1991). Preparation of cellulose 1-C-13 acetates and determination of monomer composition by NMR-spectroscopy. *Macromolecules*, *24*(11), 3050–3059.

Cetin, N. S., Tingaut, P., Ozmen, N., Henry, N., Harper, D., Dadmun, M., et al. (2009). Acetylation of cellulose nanowhiskers with vinyl acetate under moderate conditions. *Macromolecular Bioscience*, *9*(10), 997–1003.

de la Motte, H., Hasani, M., Brelid, H., & Westman, G. (2011). Molecular characterization of hydrolyzed cationized nanocrystalline cellulose, cotton cellulose and softwood kraft pulp using high resolution 1D and 2D NMR. *Carbohydrate Polymers*, *85*(4), 738–746.

Elkafrawy, A. (1982). Investigation of the cellulose LiCl dimethylacetamide and cellulose LiCl N-methyl-2-pyrrolidinone solutions by C-13 NMR-spectroscopy. *Journal of Applied Polymer Science*, *27*(7), 2435–2443.

Fujisawa, S., Okita, Y., Saito, T., Togawa, E., & Isogai, A. (2011). Formation of N-acylureas on the surface of TEMPO-oxidized cellulose nanofibril with carbodiimide in DMF. *Cellulose*, *18*(5), 1191–1199.

Gagnaire, D., Mancier, D., & Vincendon, M. (1980). Cellulose organic solutions – nuclear magnetic resonance investigation. *Journal of Polymer Science Part a-Polymer Chemistry*, *18*(1), 13–25.

Goetz, L., Foston, M., Mathew, A. P., Oksman, K., & Ragauskas, A. J. (2010). Poly(methyl vinyl ether-co-maleic acid)-polyethylene glycol nanocomposites cross-linked in situ with cellulose nanowhiskers. *Biomacromolecules*, *11*(10), 2660–2666.

Grzesiek, S., Cordier, F., Jaravine, V., & Barfield, M. (2004). Insights into biomolecular hydrogen bonds from hydrogen bond scalar couplings. *Progress in Nuclear Magnetic Resonance Spectroscopy*, *45*(3–4), 275–300.

Habibi, Y., Lucia, L. A., & Rojas, O. J. (2010). Cellulose nanocrystals: Chemistry, self-assembly, and applications. *Chemical Reviews*, *110*(6), 3479–3500.

Hirota, M., Tamura, N., Saito, T., & Isogai, A. (2009). Oxidation of regenerated cellulose with $NaClO_2$ catalyzed by TEMPO and NaClO under acid-neutral conditions. *Carbohydrate Polymers*, *78*(2), 330–335.

Hostetler, M. J., Wingate, J. E., Zhong, C. J., Harris, J. E., Vachet, R. W., Clark, M. R., et al. (1998). Alkanethiolate gold cluster molecules with core diameters from 1.5 to 5.2 nm: Core and monolayer properties as a function of core size. *Langmuir*, *14*(1), 17–30.

Huang, W. J., Fernando, S., Allard, L. F., & Sun, Y. P. (2003). Solubilization of single-walled carbon nanotubes with diamine-terminated oligomeric poly(ethylene glycol) in different functionalization reactions. *Nano Letters*, *3*(4), 565–568.

Isogai, A. (1997). NMR analysis of cellulose dissolved in aqueous NaOH solutions. *Cellulose*, *4*(2), 99–107.

Isogai, A., Saito, T., & Fukuzumi, H. (2011). TEMPO-oxidized cellulose nanofibers. *Nanoscale*, *3*(1), 71–85.

Jiang, F., Esker, A. R., & Roman, M. (2010). Acid-catalyzed and solvolytic desulfation of H_2SO_4-hydrolyzed cellulose nanocrystals. *Langmuir*, *26*(23), 17919–17925.

Jiang, F., Han, S., & Hsieh, Y.-L. (2013). Controlled defibrillation of rice straw cellulose and self-assembly of cellulose nanofibrils into highly crystalline fibrous materials. *RSC Advance*, *3*, 12366–12375.

Jiang, F., & Hsieh, Y.-L. (2013). Chemically and mechanically isolated nanocellulose and their self-assembled structures. *Carbohydrate Polymers*, *95*, 32–40.

Klemm, D., Kramer, F., Moritz, S., Lindstrom, T., Ankerfors, M., Gray, D., et al. (2011). Nanocelluloses: A new family of nature-based materials. *Angewandte Chemie-International Edition*, *50*(24), 5438–5466.

Kowsaka, K., Okajima, K., & Kamide, K. (1988). Two-dimensional nuclear magnetic-resonance spectra of cellulose and cellulose triacetate. *Polymer Journal*, *20*(12), 1091–1099.

Lu, P., & Hsieh, Y.-L. (2011). Preparation and characterization of cellulose nanocrystals from rice straw. *Carbohydrate Polymers*.

Mao, L. S., Ma, P., Law, K., Daneault, C., & Brouillette, F. (2010). Studies on kinetics and reuse of spent liquor in the TEMPO-mediated selective oxidation of mechanical pulp. *Industrial & Engineering Chemistry Research*, *49*(1), 113–116.

Montanari, S., Rountani, M., Heux, L., & Vignon, M. R. (2005). Topochemistry of carboxylated cellulose nanocrystals resulting from TEMPO-mediated oxidation. *Macromolecules*, *38*(5), 1665–1671.

Moulthrop, J. S., Swatloski, R. P., Moyna, G., & Rogers, R. D. (2005). High-resolution C-13 NMR studies of cellulose and cellulose oligomers in ionic liquid solutions. *Chemical Communications*, (12), 1557–1559.

Nardin, R., & Vincendon, M. (1986). Homonuclear and heteronuclear two-dimensional correlated nuclear-magnetic-resonance spectra of cellulose. *Macromolecules*, *19*(9), 2452–2454.

Nehls, I., Wagenknecht, W., Philipp, B., & Stscherbina, D. (1994). Characterization of cellulose and cellulose derivatives in solution by high-resolution C-13-NMR spectroscopy. *Progress in Polymer Science*, *19*(1), 29–78.

Okita, Y., Saito, T., & Isogai, A. (2010). Entire surface oxidation of various cellulose microfibrils by TEMPO-mediated oxidation. *Biomacromolecules*, *11*(6), 1696–1700.

Paakko, M., Ankerfors, M., Kosonen, H., Nykanen, A., Ahola, S., Osterberg, M., et al. (2007). Enzymatic hydrolysis combined with mechanical shearing and high-pressure homogenization for nanoscale cellulose fibrils and strong gels. *Biomacromolecules*, *8*(6), 1934–1941.

Saito, T., & Isogai, A. (2004). TEMPO-mediated oxidation of native cellulose. The effect of oxidation conditions on chemical and crystal structures of the water-insoluble fractions. *Biomacromolecules*, *5*(5), 1983–1989.

Segal, L., Creely, J. J., Martin, A. E., Jr., & Conrad, C. M. (1959). An empirical method for estimating the degree of crystallinity of native cellulose using the X-ray diffractometer. *Textile Research Journal*, *29*, 786–794.

Shibata, I., & Isogai, A. (2003). Nitroxide-mediated oxidation of cellulose using TEMPO derivatives: HPSEC and NMR analyses of the oxidized products. *Cellulose*, *10*(4), 335–341.

Sun, Y. P., Fu, K. F., Lin, Y., & Huang, W. J. (2002). Functionalized carbon nanotubes: Properties and applications. *Accounts of Chemical Research*, *35*(12), 1096–1104.

Tahiri, C., & Vignon, M. R. (2000). TEMPO-oxidation of cellulose: Synthesis and characterisation of polyglucuronans. *Cellulose*, *7*(2), 177–188.

Tang, B. Z., & Xu, H. Y. (1999). Preparation, alignment, and optical properties of soluble poly(phenylacetylene)-wrapped carbon nanotubes. *Macromolecules*, *32*(8), 2569–2576.

Terrill, R. H., Postlethwaite, T. A., Chen, C. H., Poon, C. D., Terzis, A., Chen, A. D., et al. (1995). Monolayers in three dimensions: NMR, SAXS, thermal, and electron hopping studies of alkanethiol stabilized gold clusters. *Journal of the American Chemical Society*, *117*(50), 12537–12548.

Uetani, K., & Yano, H. (2011). Nanofibrillation of wood pulp using a high-speed blender. *Biomacromolecules*, *12*(2), 348–353.

Yuan, H. H., Nishiyama, Y., Wada, M., & Kuga, S. (2006). Surface acylation of cellulose whiskers by drying aqueous emulsion. *Biomacromolecules*, *7*(3), 696–700.

Zhou, H. Y., Du, F. F., Li, X., Zhang, B., Li, W., & Yan, B. (2008). Characterization of organic molecules attached to gold nanoparticle surface using high resolution magic angle spinning H-1 NMR. *Journal of Physical Chemistry C*, *112*(49), 19360–19366.